Microsyst Technol (2014) 20:1891–1898
DOI 10.1007/s00542-013-1968-8

TECHNICAL PAPER

Challenges with high aspect ratio nanoimprint

Hella-Christin Scheer · A. Mayer · K. Dhima · S. Wang · C. Steinberg

Received: 14 June 2013 / Accepted: 5 November 2013 / Published online: 23 November 2013

Abstract When nanoimprint is not used for lithography purposes (NIL), but for the direct patterning of polymeric layers, high aspect ratio patterns may be of interest for a number of applications. The definition of such patterns in a nanoimprint process deals with two aspects, a successful filling of the high aspect ratio cavities of the stamp used, followed by a successful separation of the high aspect ratio structures defined in the polymeric layer on the substrate, from the stamp. These two aspects are addressed by shedding light to the impact of capillary effects during the filling of high aspect ratio cavities, and to the deformation processes involved in the separation of the stamp from the polymeric structures, where adhesional energies have to be overcome without cohesional failure. Both aspects are discussed in terms of the geometries involved, the stamp geometries as well as the polymeric layer thickness, and correlations with thermally-assisted (T-NIL) and UV-assisted (UV-NIL) processing are deduced. The aspects discussed are typical of a nanoimprint situation with thin polymeric layers on hard substrates.

1 Introduction

Nanoimprint (NIL, nanoimprint lithography, Chou et al. 1996; Guo 2004; Schift 2008) has the ability to define nanometer-scaled patterns over large areas in parallel, and a lot of examples have already demonstrated its potential for applications in photonics, microsystems, microelectronics and patterned media. It is not only suitable as a lithography technique (to define an intermediate mask on a substrate for further processing), but also for the direct patterning of functional surfaces, e.g. for optical purposes [light guiding (Weiss et al. 2010), anti-reflection] as well as for device preparation in the field of organic electronics (Cedeno et al. 2002) or photovoltaics, where large area processing is asked for. Beyond planar processing also roll-to-roll or roll-to-flat processing have already been demonstrated (Taniguchi et al. 2011), opening routes inaccessible to conventional processing customary in microelectronics.

Though offering the benefit of avoiding typical lithography limitations like diffraction and proximity effects, nanoimprint, as a mechanically based patterning technique, features restrictions related to its mechanical nature. It is a contact technique, so anti-adhesive layers, their application and their durability (Schift et al. 2005; Garidel et al. 2007; Scheer et al. 2008), are essential for a successful pattern definition. Moreover, with high aspect ratio structures, the challenge increases dramatically (Hirai et al. 2003a, b), as the stamp contact area (where easy separation is required after the process) is large compared to the respective substrate area (where good adhesion is demanded). The latter is a consequence of the fact, that nanoimprint typically is performed with thin polymeric layers (some 100 nm) on hard substrates, in contrast to typical hot embossing of polymeric films of some 100 μm thickness. There, prevention of adhesion to the stamp is of primary importance; good film adhesion to the bottom tooling can be provided by gluing or by selective roughening of the tool surface, and the relatively thick polymeric film is able to compensate some of the stress occurring during separation by elastic deformation. With nanoimprint, in contrast, the thin layers between the hard surfaces (substrate and mold) provide only small compensation of forces so that

H.-C. Scheer (✉) · A. Mayer · K. Dhima · S. Wang · C. Steinberg
Microstructure Engineering, Department E: Electrical, Information and Media Engineering, University of Wuppertal, Rainer-Gruenther-Str. 21, 42119 Wuppertal, Germany
e-mail: scheer@uni-wuppertal.de

adhesion to stamp and surface are most critical for separation. Guidelines derived for macroscopic processing (Zosel 1985) should be observed to facilitate separation, but in a real nanoimprint process they are applicable only in parts: The choice of a separation temperature above room temperature is often applied (typically with nanoimprint the pressure release occurs at 20–30 °C below T_g, the glass transition temperature) in order to make use of the mobility of secondary relaxation processes with polymers (van Krevelen 1990); separation at low temperature (to make use of thermal shrink for separation) is limited, as a typical imprint stack in thermal nanoimprint has low mass and thus low heat capacity, and as most often a manual separation is performed. A low separation velocity, decreasing the adhesional forces to be overcome, is beneficial; however, with typical structure heights in the micrometer-regime and below, realization is hardly possible.

With high aspect ratio structures also the filling of the stamp cavities in NIL may be challenging. A number of simulations have addressed this issue, where nanoimprint as a mechanical patterning technique highly depends on the geometries involved. Rowland et al. (2005) e.g. found that with narrow cavities the time required for filling is substantially increased (compared to wider cavities), in particular when the stamp patterns are high. This is a consequence of the primarily lateral squeeze-in of polymeric material into the cavities, induced by the thin layers involved. Filling of high aspect ratio cavities is thus hampered, as a displacement of the polymer in vertical direction is required. Other simulations by e.g. Jeong et al. (2002) have shown that for the filling of high aspect ratio, narrow cavities also surface tension effects (capillary forces) are of impact. Both simulations assume continuum properties of the materials, thus, with polymers, they are no more applicable when the dimensions of the molecules are in the range of the stamp geometries involved. Taking the radius of gyration R_g (Strobl 1997) of a linear chain molecule as a reference, molecular size effects have to be expected with stamp geometries in the range of 10 nm (typical imprint polymers feature 10^2–10^3 monomers per chain). Molecular dynamics simulations with oligomers have shown (Taga et al. 2010) that with molecular sizes in the range of the cavity size the forces required to fill the cavities increase substantially beyond those expected from continuum mechanics simulations.

This contribution addresses two aspects related to high aspect ratio imprint, (1) the filling of high aspect ratio cavities and (2) the separation of high aspect ratio structures from the stamp. In order to elaborate basic issues, simplified model assumptions are used, easily described by analytical relations. By discussing the physical impact of these relations it will be shown that compromises are required to obtain both, successful filling and successful separation as well. With filling, capillary effects are addressed; with separation, the deformation of the structures in context with adhesion and cohesion is discussed. Both aspects are addressed in view of T-NIL (thermal nanoimprint) as well as UV-NIL (UV assisted nanoimprint), the two main nanoimprint techniques applicable for the definition of high aspect ratio structures.

2 Filling of high aspect ratio stamp cavities

Filling of high aspect ratio stamp cavities relies on both, the squeezing of polymeric material from below the adjacent elevated stamp structures into the cavity, proceeding under the external pressure applied, p_{ext}, as well as on capillary effects related to the polymer-air interface in the cavities, specified by the Laplace pressure Δp_{LA}. The latter is a pressure jump across the interface, the difference between the pressure in the liquid (the polymer), p_L, and the pressure in the gas phase (the air), p_G, at the interface location. This pressure difference differs from zero with curved interfaces only, its height being directly related with the (2-dimensional) curvature of the interface, κ, and the geometries of the capillary. In case of a circular capillary of radius R it amounts to

$$\Delta p_{LA} = p_G - p_L = \gamma \cdot \kappa = \gamma \cdot \left(\frac{1}{Rki} + \frac{1}{Rkj} \right) = \gamma \cdot 2 \frac{\cos\theta}{R}, \qquad (1)$$

R_{ki} and R_{kj} being the principal radii of curvature, γ the surface tension of the liquid (the surface energy of the polymer) and θ the contact angle the liquid (polymer) forms with the capillary surface. With a linear capillary of width w, a one-dimensional curvature is obtained, with $R_{kj} = \infty$ and $R_{ki} = \cos\theta/(w/2)$; thus the situation with a linear cavity is quite similar to the situation with a dot-like or circular cavity.

Figure 1 illustrates the situation; as contact angles in the range $0° < \theta < 180°$ are generally possible, two situations may occur; either the polymer wets the capillary ($\theta < 90°$) or it does not ($\theta > 90°$). With a contact angle $\theta = 90°$ the Laplace pressure changes sign, being positive below 90° and negative above 90°. In the first case, the Laplace pressure aids to fill the cavity—this is the most preferred situation. In the latter case the Laplace pressure opposes cavity filling (assuming an intended filling of the cavity in vertical direction z). Filling of the capillary requires a pressure drop within the polymer in z-direction, similar to a flow through a pipe (radius R, length L), where the mean velocity of flow (with a parabolic velocity distribution across the diameter) is given by

$$\bar{v} = \frac{1}{3\eta} R^2 \cdot \frac{\Delta p}{L}, \qquad (2)$$

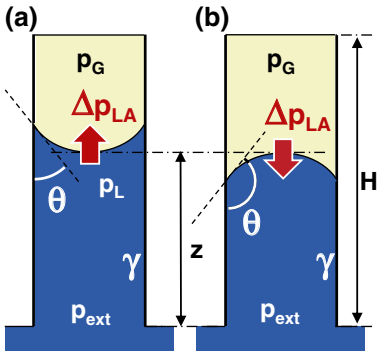

Fig. 1 Situations with filling of vertical capillaries (no gravity); with $\theta < 90°$ the capillary is wetted by the polymer (**a**), with $\theta > 90°$ it is not (**b**). The Laplace pressure across the interface is indicated by the *arrows*. With closed capillaries as typical of T-NIL and UV-NIL (stamp structure height H) the pressures within the gas phase (p_G) and in the liquid phase (p_L, p_{ext}) are substantially different with both situations (see text)

with p the local pressure, $\Delta p/L$ the pressure difference across the tube length and η the viscosity of the fluid. With nanoimprint, the respective pressure drop is the difference between the pressure in the polymer at the bottom of the cavity (as obtained from the external pressure applied p_{ext}) and the respective pressure p_L at the interface, acting across the height z. (With the microscopic geometries involved here gravity can be neglected.)

When hard stamps are used with T-NIL and UV-NIL, the situation is even more complicated, as the capillaries are closed ones. (With soft stamp materials (Suh et al. 2009), featuring permeability for gases, the situation is less critical, in particular when long processing times are provided, allowing the enclosed gas to diffuse through the stamp.) With a closed capillary, compression of the gas phase may occur, as the pressure within the gas is defined by Eq. 1 again, with

$$p_G = p_L + \Delta p_{LA} \approx p_L + 2\gamma \frac{\cos\theta}{R}, \tag{3}$$

the latter relationship being exact only without deformation of the interface—for a simplification of the arguments such an assumption is made, stating that the interface still represents a spherical surface. Furthermore, any change of the surface energy and contact angle due to pressure is ignored.

Equation 3 then states that with a wetted capillary the pressure in the gas phase is higher than in the liquid, so that, in a combined effect of p_{ext} and Δp_{LA}, $(p_{ext} + \Delta p_{LA})$, the gas is compressed, resulting in a self-acting suction of the polymer in vertical direction into the capillary. In contrast, in the non-wetting situation, the gas phase is at a pressure lower than the liquid and will be hardly compressed. Then, a filling of the capillaries is only possible with $(p_{ext} - \Delta p_{LA}) > 0$. When the external pressure is low, as it is the case with UV-NIL, then the polymer is unable to enter the capillary due to the negative contribution of Δp_{La}. Only with high external pressures as used in T-NIL a cavity filling against the Laplace pressure is possible.

As the Laplace pressure increases with decreasing cavity width the effect becomes more pronounced with small geometries. To give an estimate, a maximum Laplace pressure (with $\gamma \approx 30$ mN/m) of about 0.5 bar will be reached with a capillary of 1 μm radius, whereas with a 10 nm capillary a value of 50 bar is obtained, a pressure in the range of typical processing pressures with T-NIL. These values indicate that T-NIL may be able to provide filling even in situations under non-wetting conditions, as long as the cavities are not too small. In the non-wetting case, the filling of cavities with T-NIL becomes the more limited the smaller the cavities, and cavities of some 10 nm may not become filled. With UV-NIL, no cavity filling at all is possible in the non-wetting case. UV-NIL has ultimately to rely on wetting and the support of the capillary action for a filling of cavities. But due to the geometry dependence of the Laplace pressure, this support is high for small cavities only, micrometer-sized cavities remain unfilled, those are filled with non-compressed gas. Only with increased processing times the gas remaining in the cavities will diffuse into the polymer, thus enabling cavity filling in an indirect way. But in-diffusion is a timely process, in particular with low temperature and low pressure, as it is the case in UV-NIL. These issues suggest an evacuation of the processing chamber to improve the filling situation with UV-NIL, a measure applicable for UV-NIL with spin-coated layers only. With a dispensed liquid resist evacuation may be in conflict with resist evaporation. To solve this problem it was proposed to exchange the air against a special gas that condenses at a low over-pressure, so that a filling of the cavities is provided by the collapse of the gas volume in the cavities (Hiroshima and Komuro 2007).

Nonetheless, for T-NIL and for UV-NIL as well, a wetting situation is the more beneficial one for cavity filling. Unfortunately, the wetting situation opposes an easy separation, as addressed below.

3 Separation of high aspect ratio stamp structures

To illustrate the situation during the separation of sample and stamp, again a simplified view is assumed as sketched in Fig. 2. The stamp is assumed to feature vertical sidewalls, with no surface roughness. Without surface roughness, adhesion between two materials (without chemical bonding) under normal forces is adequately described by the thermodynamic work of adhesion (adhesional energy per area), w_{adh}, in particular under very slow separation velocities. Successful separation requires an energy

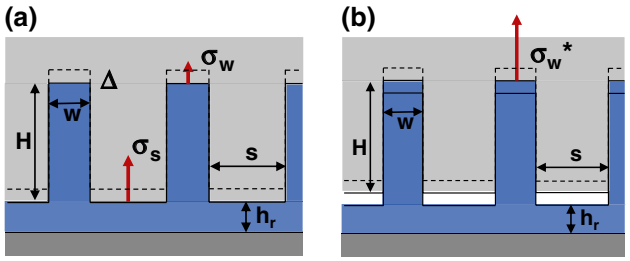

Fig. 2 Sketch of situations during separation of the imprinted structures from the stamp. The separation is assumed to start with fully filled cavities. **a** Definition of geometries (stamp with pattern size s, cavity width w and height H; h_r, residual layer remaining in the polymer) as well as normal stresses within the polymer in the region of elevated stamp structures, σ_S, and in the cavity region, σ_W. A movement of the (rigid) stamp by Δ in vertical direction is indicated by the *dashed line*. **b** Situation after separation within the elevated stamp pattern region. The stress in the cavity region has increased compared to (**a**), see text

exceeding w_{adh}, which, however, does not disrupt the polymeric material. Furthermore, with a uniform material without voids, cohesion is adequately described by the thermodynamic work of cohesion (cohesional energy per area), w_{coh}. Simplifying further the interaction between the materials to be primarily caused by non-polar van der Waals forces (Lorenz forces, Israelachvili 2011), adhesional and cohesional energies are given by

$$w_{adh} = 2\sqrt{\gamma_s \gamma_p} \quad \text{and} \quad w_{coh} = 2 \cdot \gamma_p, \tag{4}$$

with γ_p the surface tension of the polymer and γ_s the surface energy of the surface in contact with the polymer (the stamp or the substrate), both at separation temperature. The adhesional energy (two dis-similar surfaces in contact) is described here in correspondence to the cohesional energy (two similar surfaces in contact) by the geometric mean of the surface energies of the two materials involved, following Fowkes (Good 1992). Figure 3a illustrates Eq. 4, giving the adhesional energy of a polymer (surface tension 40 mN/m) to a surface of varying surface energy γ_s. The cohesional energy (80 mJ/m^2) is indicated.

With a typical, well-prepared (de-hydration baked) imprint substrate (Si, oxide) the surface energy is high (80–100 mJ/cm^2), resulting in a high value for w_{adh} to the substrate, a beneficial situation to overcome adhesional failure there. However, in order to provide preferential separation at the stamp-polymer-interface, the surface energy of the stamp (often prepared from similar materials as the substrate) has to be decreased substantially. Typically, values of $\gamma_s \leq 20$ mJ/cm^2 are obtainable when anti-sticking layers are applied (Beck et al. 2002; Jung et al. 2005; Schift et al. 2005). The lower the surface energy of the stamp the lower the adhesion.

Unfortunately, a low surface energy comes along with a non-wetting situation of the stamp cavities. Under the above made assumptions the contact angle follows the relationship

$$\cos\theta = 2\sqrt{\frac{\gamma_s}{\gamma_p}} - 1. \tag{5}$$

The contact angle θ according to this relationship is indicated by the broken lines in Fig. 3b, considering a filling of the stamp cavities at similar temperature (as typical for UV-NIL) and at elevated temperature compared to separation (as typical for T-NIL). A contact angle $\theta \geq 90°$ indicates the transition from a wetting to a non-wetting situation. With UV-NIL, relying ultimately on wetting for a filling of the capillaries, this restricts the regime of 'beneficial' stamp surface energies to values of $\gamma_s > 10$–15 mJ/m^2. With T-NIL, as discussed above, a filling of cavities can be obtained with even larger contact angles, the only limit

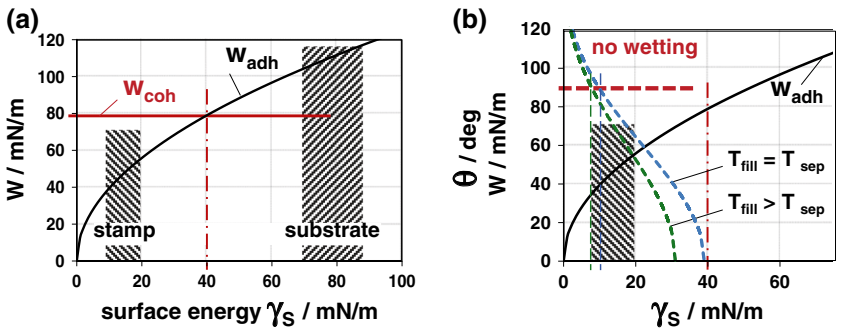

Fig. 3 Adhesional energy of a polymer (surface tension 40 mN/m) to a surface of varying surface energy γ_s. The adhesion increases with increasing surface energy. **a** Situations typical of the substrate contact and the stamp contact are marked by the *vertical bars*. Successful separation requires a cohesional energy that is higher than the adhesional energy to the stamp, as well as a preferential (high) adhesion to the substrate. **b** Detail within the range of low surface energy: adhesional energy to the stamp and contact angle. For the contact angle an equal temperature is assumed for filling of the cavities and for separation ($T_{fill} = T_{sep}$, similar to UV-NIL) as well as an elevated temperature ($T_{fill} > T_{sep}$, similar to T-NIL)

for the stamp surface energy is given by the deposition process of the anti-sticking layers and its physics. Typical values obtainable with silane-based anti-sticking agents are in the range of 10 mJ/m^2 < γ_s < 20 mJ/m^2 (Jung et al. 2005), where a careful estimation of the evaluated values is required in order not to mis-interprete a rough surface, that typically develops with thick layers. Thin anti-sticking layers chemically bonded to the surface (as envisaged for long-term stability) are most often incomplete, disordered monolayers (Scheer et al. 2008). Thus, with T-NIL the situation is less critical than with UV-NIL, because the cavity filling and the separation typically proceed at different temperatures (and contact angles and surface energies typically decrease with increasing temperature).

For a further discussion of the separation process, let us assume a typical imprint situation with γ_p = 30–40 mN/m (w_{coh} = 60–80 mJ/m^2) and γ_s = 15–20 mJ/m^2 (w_{adh} = 42–56 mJ/m^2) for the stamp; the ratio between the cohesional and adhesional energies per area then amounts to 1.2–1.4. Furthermore, let us assume that the stamp shown in Fig. 2a is moved by some distance Δ in vertical direction as indicated, as a consequence of an external separation force applied. Without stamp roughness, the movement provides shear forces along the stamp sidewalls only, thus no friction occurs; the separation force acts in vertical direction, resulting in normal stresses (force per area), σ_S within the elevated stamp area and σ_W within the cavity area of the stamp. For further simplification, let us restrict the discussion to a single period ($s + w$) of a periodic pattern, with a pattern size s of the stamp and a cavity width w, as indicated in Fig. 2a.

In the initial situation the polymer adheres to the stamp and to the substrate surface, so that any movement of the stamp by Δ results in a deformation of the polymeric layer (stamp and substrate deform much less and are assumed rigid). Furthermore, as the stress required to deform a layer by the same amount Δ is larger with thin layers than with thick layers, the normal stress in the elevated stamp region is higher than in the cavity region, $\sigma_S > \sigma_W$. The same applies to the deformational energy per area, w_{def}, which can be described by

$$w_{def} = \frac{1}{A} W_{def} = \frac{1}{A} \cdot \frac{1}{2} \sigma \cdot \varepsilon \cdot V = \frac{1}{2} \sigma \cdot \Delta, \tag{6}$$

with W_{def} being the total energy of deformation and assuming small deformations only with ε, the strain, (representing the relative deformation occurring, here $\varepsilon = \Delta/h$), with h the respective layer thickness and the volume involved $V = Ah$. As a consequence from Eq. 6, under our conditions with Δ = const the deformational energies per area differ by the same factor, a, as the respective stresses,

$$W_{def,S} : W_{def,W} = \sigma_S : \sigma_W = (H + h_r) : h_r = \mathrm{a}. \tag{7}$$

It should be mentioned that the assumption of small strain (Hooke's law) used here does not restrict the statements. Admittedly, with polymers a large strain situation may be already met at small stresses. In that case the stress is usually assumed to be proportional to the strain ratio (or extension ratio), λ, with $\lambda = (h + \Delta)/h$ in terms of the parameters used here. As λ and ε are related by $\varepsilon = 1 + \lambda$, the last factor ($\Delta$) in Eq. 6 would simply have to be replaced by $(h + \Delta)$ to account for large strain. The general arguments used are not affected by this change.

Based on these arguments and based on the fact, that a mean normal stress may be defined as.

$$\bar{\sigma} = \frac{s \cdot \sigma_S + w \cdot \sigma_W}{s + w}, \tag{8}$$

the stresses within the cavity region and in the elevated stamp region can be expressed by

$$\sigma_W = \bar{\sigma} \cdot \frac{b+1}{\mathrm{a}b+1} \quad \text{and} \quad \sigma_S = \mathrm{a} \cdot \sigma_W = \sigma_W \cdot \frac{h_r + H}{h_r} = \sigma_W \left(1 + \frac{H}{h_r}\right), \text{ with } b = \frac{s}{W}. \tag{9}$$

Equations 7 and 9 are of general impact for the separation process, as they result in a specific separation sequence. Separation of the stamp from the polymer is obtained, when the deformation energy provided to the polymer by the stamp movement Δ exceeds the adhesional energy, w_{adh}. This situation is first met within the elevated stamp regions (see Fig. 2b), where the stress is higher than in the cavities, namely for $w_{def,S} > w_{adh}$. Upon separation within s, the stress σ_S drops to zero, so that the mean stress now acts on the cavity region w only, resulting in a jump of the cavity stress from its initial (small) value σ_W to

$$\sigma_W^* = \bar{\sigma} \cdot \frac{W+S}{W} = \bar{\sigma} \left(1 + \frac{S}{W}\right). \tag{10}$$

What follows depends on the size of this jump in stress. In case that σ_W* gives rise to a deformation energy per area of w_{def}* > w_{adh}, the cavity region becomes separated, too. But in case that σ_w* results in a deformation energy per area of w_{def}* > w_{coh}, the polymer layer becomes disrupted and cohesional failure occurs. Assuming some slight fixing of the polymer to the cavity walls, the region most prone to cohesional failure is the bottom of the structures, as a strong local deformation occurs there during spring-back of the residual layer. Such a rip-off at the bottom of the structures can often be observed experimentally (Hirai et al. 2003a, b).

Figure 4 illustrates the separation process by indicating the stresses ($\sigma_S, \sigma_W, \bar{\sigma}, \sigma_W^*$) and the energies per area involved (w_{adh}, w_{coh}) with an ongoing progress of separation, indicated by a linear increase in Δ. The adhesional

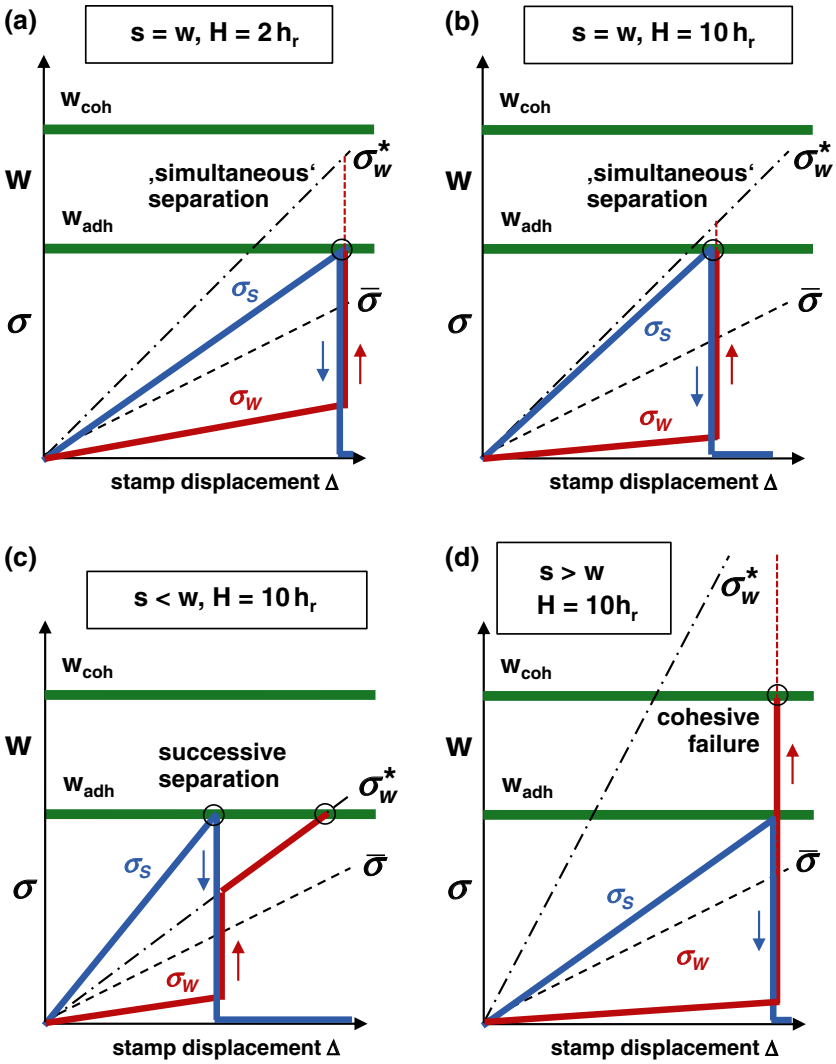

Fig. 4 Visualization of a separation process, illustrated by the stresses involved (see text) increasing with increasing displacement of the stamp Δ. A similar mean stress (due to an external separation force) is assumed. The cohesional and adhesional energies per area are indicated, defining the ultimate stress values for adhesional failure (successful separation) and cohesional failure (rupture). (Calculations for linear stamp geometry. For transfer to other stamp geometries see text.) **a** Equal line and space width ($s = w$), low stamp height ($H = 2\ h$): Low dynamic loading, simultaneous separation. **b** Equal line and space width ($s = w$), high stamp height ($H = 10$ h): Increased dynamic loading, simultaneous separation. **c** Decreased stamp line width ($2\ s = w$), high stamp height ($H = 10$ h): Low dynamic loading, successive separation. **d** Increased stamp line width ($s = 2w$), high stamp height ($H = 10$ h): high dynamic loading, cohesional failure

and cohesional energies differ by a factor of about 1.4, according to the simplifying assumptions made. The ratios $s{:}w$ and $H{:}h_r$ are varied.

Figure 4a refers to $s = w$ and a small stamp height, $H = 2\ h$. When the elevated stamp structures separate from the stamp at some displacement Δ, the stress in the cavity region jumps to σ_W^*; but as this stress results in a deformation energy beyond w_{adh}, the cavity region separates from the stamp, too, almost simultaneously with the elevated stamp region. With an increased height of the stamp (Fig. 4b), $H = 10\ h$, the separation proceeds similarly, however, separation occurs at a lower displacement Δ, due to the increased factor between σ_S and σ_W. As σ_W is lower than in case a, the jump occurring to σ_W^* is higher, which results in a higher dynamic loading to the polymer at the time the jump occurs.

Figure 4c refers to a changed duty cycle of the stamp, $2s = w$, and $H = 10$ h as before. As the ratio s/w alters the maximum stress in the cavity region after the first separation, σ_W^*, this limiting value is reduced, it amounts to 1.5 times the mean value here. Therefore, when separation occurs in the elevated stamp area, the jump in the cavity stress to σ_W^* results in a deformation energy still below the adhesion limit; thus a further increase in Δ is required to separate the cavity region of the stamp, as indicated. The case $s < w$ obviously results in a successive separation, first in the elevated stamp regions, then in the cavities.

Figure 4d finally refers to the most critical situation, $s > w$, the values $s = 2w$ and $H = 10\ h$ are chosen here. When separation is met with the elevated stamp region, the jump of the stress within the cavities may result in a deformation energy exceeding the cohesional energy per area, w_{coh}, so that cohesional failure occurs. (Even with cohesional energies higher than the one assumed here on the basis of non-polar van der Waals forces, the argument holds, due to the high value of σ_W^*.)

These simple arguments indicate that due to the specific difference in stress occurring in elevated stamp regions

and cavity regions, the separation of stamps with structures $s > w$ is most critical, whereas at $s \leq w$ the risk for cohesional failure is much lower, in particular with $s \ll w$; dynamic loading increases with increasing ratio of stamp height to residual layer height, H/h_r. A direct correlation with the aspect ratio of the imprinted structures, H/w, is not possible, as the residual height remaining, h_r, is of impact.

This separation behaviour again differentiates the imprint process compared to an embossing process. With embossing, the factor H/h_r is small, so that the stresses acting in the elevated stamp regions and in the cavities are (almost) equal, and the different situations illustrated in Fig. 4 are hardly observed, in particular as other effects (thermal shrink, surface roughness, etc.) may cover them.

With imprint, too, thermal shrink (with T-NIL) or curing shrink with (UV-NIL), both in the same range, will alter the separation process. With excellent anti-sticking layers, a gap may develop between stamp and polymer in the cavity region, so that separation of the elevated stamp region is required only, and thus separation is performed easily (Shibata et al. 2010). Even without a gap, the tensional stresses in the polymer within the stamp cavities have the same direction as the ones induced by an external separation force, thus assisting separation. The situation would be similar as in Fig. 4, the main difference being that the separation already occurs at lower values of external stamp displacement Δ. With high shrinkage stress in vertical direction, as expected with high aspect ratio patterns, successive separation may occur in reversed order, first aseparation in the cavity regime and then in the elevated stamp region. The respective behaviour may simply be estimated from Fig. 4 by adding a constant (shrink-induced) pre-stress σ_0 to the stresses resulting from the stamp movement Δ. A stress induced by shrink is proportional to the volume and thus proportional to the respective polymer height. Thus the shrink-induced stress in the elevated stamp region is lower than in the cavity region, $\sigma_{S0} < \sigma_{W0}$, with $\sigma_{W0} = a\sigma_{S0}$, in contrast to theseparation-induced stresses (Eq. 9). Thus an effective shrink-induced stress σ_0 has to be added in the cavity region to account for this situation with

$$\sigma_0 = \sigma_{W0} - \sigma_{S0} = (a - 1)\sigma_{S0} \propto H \cdot S, \tag{11}$$

S being the shrink factor ($S < 1$) and H the stamp structure height, as before.

Stamp roughness, however, changes the situation, for filling the cavities as well as for separation after imprint. With primarily vertical roughness (as obtained with stamp preparation by lithography and RIE (reactive ion etching)) filling may be enhanced by wicking (Bico et al. 2001) within the open, vertical capillaries along the stamp sidewalls, whereas horizontal grooves (as obtained with stamp preparation by deep reactive ion etching in a BOSCH-process (e.g. Sakamoto et al. 2011) may modulate the surface shape, pinning at the ridges hindering cavity filling (Mayer 2012). During separation, any roughness increases the surface area and may result in local normal forces along the sidewalls and thus frictional effects, in particular with horizontal grooves. These frictional effects are especially important in situations with high aspect ratio structures, where the stamp cavities are narrowand comparable to the roughness (Hirai et al. 2003a, b). The separation process may then result in a permanent deformation of the structures (over-expansion) as long as the cohesional energy is not exceeded.

Although the calculation presented in Fig. 4 is based on the assumption of linear stamp geometries from Eq. 8 on, a transfer to arbitrary periodic patterns (e.g. dot patterns) is easy. Then the 'weighting factors' for the stresses are not the geometries s and w, but the respective areas, A_s and A_w (elevated area of stamp pattern and cavity area), and Eq. 8 changes to.

$$\bar{\sigma} = \frac{A_S \cdot \sigma_S + A_W \cdot \sigma_W}{A_S + A_W}. \tag{12}$$

Accordingly, as a similar mean stress $\bar{\sigma}$ has to be considered to compare the linear situation with e.g. a dot pattern, the only change will be the size of σ_w and σ_s compared to $\bar{\sigma}$. Consequently, in case of a checkerboard pattern ($s = w$ and $A_s = A_w$) the situation is identical to Fig. 4a, b. In case of a stamp with a dot pattern ($s < w$) or a stamp with a hole pattern ($s > w$) the effect is stronger than the one for a stamp with linear geometries (Fig. 4c, d). In particular, with a hole pattern of the stamp (imprinted isolated polymeric pillars) the risk for cohesional failure (Fig. 4d) is extremely high, as the sharp rise of σ_w increases in magnitude (due to the higher value of σ_w^*).

Furthermore, the considerations may also be applied to more realistic stamps with inclined sidewalls. With inclined sidewalls the polymeric deformation increases in magnitude from the top of the sidewall ($\varepsilon(\sigma_w) = \varepsilon_{min}$) to the bottom of the sidewall ($\varepsilon(\sigma_s) = \varepsilon_{max}$), corresponding to the local sidewall slope, so that all values between σ_s and σ_w exist somewhere along the sidewall. With a small slope (almost vertical) of the sidewall only, Eqs. 8 and 12 are still applicable and any friction along the sidewalls during separation can safely be neglected. With a sidewall slope of decreasing magnitude (increasing inclination) the sharp drop of σ_s (and sharp rise of σ_w) upon reaching w_{adh} in Fig. 4 will proceed more and more gently the more inclined the sidewall is. A correct calculation then requires including (adding) a third contribution in Eq. 12 to cover the projected area of the sidewalls. This third contribution may even be used to cover surface roughness of the sidewalls due to lithography and etching, which often results in vertical corrugations. Such corrugations increase the

effective area of the sidewalls without a strong contribution to friction.

4 Summary and conclusion

Simple assumptions were made to illustrate the impact of capillary action for the filling of high aspect ratio cavities as well as the separation of the respective replica from the stamp after imprint. With filling, a wetting of the stamp cavities would be beneficial. It is in particular required in cases, where only low pressures are provided in the process, as in UV-NIL. As wetting requires low contact angles, which cannot be provided with the small surface energies that are beneficial for separation, a compromise has to be found. Furthermore, as both aspects, filling of stamp cavities and separation after the process, are strongly dependent on the geometries involved, not only the stamp geometries, but also the height of the respective polymeric layers, an understanding of these geometric aspects is vital for a successful imprint of high aspect ratio structures.

References

Beck M, Graczyk M, Maximov I, Sarwe E-L, Link TGI, Keil M, Montelius L (2002) Improving stamps for 10 nm level wafer scale nanoimprint lithography. Microelectron Eng 62:441–444

Bico J, Tordeux C, Quere D (2001) Rough wetting. Europhys Lett 55:214–220

Cedeno CC, Seekamp J, Kam AP, Hoffmann T, Zankovych S, Sotomayor-Torres CM, Menozzi C, Cavallini M, Murgia M, Ruani G, Biscarini F, Behl M, Zentel R, Ahopelto J (2002) Nanoimprint lithography for organic electronics. Microelectron Eng 61–62:25–31

Chou SY, Krauss PR, Renstrom PR (1996) Nanoimprint lithography. J Vac Sci Technol B 14:4129–4133

Garidel S, Zelsman M, Chaix N, Voisin P, Boussey J, Beaurain A, Pelissier B (2007) Improved release strategy for UV nanoimprint lithography. J Vac Sci Technol B 27:2430–2434

Good RJ (1992) Contact angle, wetting and adhesion: a critical review. J Adhes Sci Technol 6:1269–1302

Guo J (2004) Recent progress in nanoimprint technology and its applications. J Phys D Appl Phys 37:R123–R141

Hirai Y, Yoshida S, Takagi N, Tanaka Y, Yabe H, Sasaki K, Sumitani H, Yamamoto K (2003a) High aspect pattern fabrication by nanoimprint lithography using fine diamond mold. Jpn J Appl Phys 42:3863–3867

Hirai Y, Yoshida S, Takagi N (2003b) Defect analysis in thermal nanoimprint lithography. J Vac Sci Technol B 21:2765–2770

Hiroshima H, Komuro M (2007) UV-nanoimprint with the assistance of gas condensation at atmospheric environmental pressure. J Vac Sci Technol B 25:2333–2336

Israelachvili JN (2011) Intermolecular and surface forces. Academic Press Elsevier, Amsterdam

Jeong J-H, Choi Y-S, Shin Y-J, Lee J–J, Park K-T, Lee E-S, Lee S-R (2002) Flow behaviour at the embossing stage of nanomprint lithography. Fibers Polym 3:113–119

Jung GY, Li Z, Wu W, Chen Y, Olnyck DL, Wang S-Y, Tong WM, Williams RS (2005) Vapor-phase self-assembled monolayer for improved mold release in nanoimprint lithography. Langmuir 21:1158–1161

Mayer A, Dhima K, Möllenbeck S, Wang S, Scheer H-C, Sakamoto J, Kawata H, Hirai Y (2012) Study of defect mechanisms in partly filled stamp cavities for thermal nanoimprint control. J Vac Sci Technol B 30:06FB03-1-06FB03-6

Rowland H, King WP, Sun A, Schunk PR (2005) Impact of polymer film thickness and cavity size on polymer flow during embossing: towards process design rules for nanoimprint lithography. J Micromech Microeng 15:2414–2425

Sakamoto J, Fujikawa N, Nishikura N, Kawata H, Yasuda M, Hirai Y (2011) High aspect ratio fine pattern transfer using a novel mold by nanoimprint lithography. J Vac Sci Technol B 29:06FC15-1-06FC15-5

Scheer H-C, Häfner W, Fiedler A, Möllenbeck S, Bogdanski N (2008) Quality assessment of antisticking layers for thermal nanoimprint. J Vac Sci Technol B26:2380–2384

Schift H (2008) Nanoimprint lithography: an old story in modern times? A review. J Vac Sci Technol B 26:458–480

Schift H, Saxer S, Park S, Padeste C, Pieles U, Gobrecht J (2005) Controlled co-evaporation of silanes for nanoimprint stamps. Nanotechnology 16:S171–S175

Shibata M, Horiba A, Nagaoka Y, Kawata H, Yasuda M, Hirai Y (2010) Process simulation system for UV-nanoimprint lithography. J Vac Sci Technol B 28:C6M108-C6M113

Strobl G (1997) The physics of polymers. Springer, Berlin

Suh K-Y, Park C, Kim P (2009) Capillary force lithography: a versatile tool for structured biomaterials interface towards cell and tissue engineering. Adv Funct Mater 19:2699–2712

Taga A, Yasuda M, Kawata H, Hirai Y (2010) Impact of molecular size on resist filling process in nanoimprint lithography: Molecular dynamics study. J Vac Sci Technol B 28:C6M68-C6M71

Taniguchi J, Unno N, Marujama H (2011) Large diameter roll mold fabrication method using a small diameter quartz roll mold and UV nanoimprint. J Vac Sci Technol B 29:06FC08-06FC11

van Krevelen DW (1990) Properties of polymers. Elsevier, Amsterdam

Weiss DN, Yuan H-C, Lee BG, Branz HM, Meyers ST, Grenville A, Keszler DA (2010) Nanoimprinting for diffractive light trapping in solar cells. J Vac Sci Technol B 28:C6M98-C6M103

Zosel A (1985) Adhesion and tack of polymers; influence of mechanical properties and surface tensions. Colloid Polymer Sci 263:541–553